STORAGE RING MEASUREMENT OF ELECTRON IMPACT IONIZATION FOR Mg^{7+} FORMING Mg^{8+}

2010 ApJ 712 1166

(http://iopscience.iop.org/0004-637X/712/2/1166)

The Astrophysical Journal, 712:1166–1171, 2010 April 1 doi:10.1088/0004-637X/712/2/1166

STORAGE RING MEASUREMENT OF ELECTRON IMPACT IONIZATION FOR Mg^{7+} FORMING Mg^{8+}

M. Hahn[1], D. Bernhardt[2], M. Lestinsky[1], A. Müller[2], O. Novotný[1], S. Schippers[2], A. Wolf[3], and D. W. Savin[1]
[1] Columbia Astrophysics Laboratory, Columbia University, 550 West 120th Street, New York, NY 10027, USA
[2] Institut für Atom- und Molekülphysik, Justus-Liebig-Universität, Leihgesterner Weg 217, 35392 Giessen, Germany
[3] Max-Planck-Institut für Kernphysik, Saupfercheckweg 1, 69117 Heidelberg, Germany
Received 2009 December 3; accepted 2010 February 2; published 2010 March 11

ABSTRACT

We report electron impact ionization cross section measurements for Mg^{7+} forming Mg^{8+} at center of mass energies from approximately 200 eV to 2000 eV. The experimental work was performed using the heavy-ion storage ring TSR located at the Max-Planck-Institut für Kernphysik in Heidelberg, Germany. We find good agreement with distorted wave calculations using both the GIPPER code of the Los Alamos Atomic Physics Code suite and using the Flexible Atomic Code.

Key words: atomic data – atomic processes – methods: laboratory

Online-only material: color figures

1. INTRODUCTION

Cosmic plasmas driven by electron impact ionization (EII) are formed in many astrophysical sources. Interpreting the thermal and ionization properties of these objects requires an accurate understanding of the charge state distribution (CSD) of the sources (Brickhouse 1996; Landi & Landini 1999; Bryans et al. 2006). The CSD calculations in turn depend on the balance between EII and electron–ion recombination and much work has been carried out in deriving the atomic data needed for reliable models (reviewed in Bryans et al. 2009).

Unfortunately, a major limitation concerning the EII data has been the difficulty of providing unambiguous experimental results due to the challenge of producing well-characterized ion beams. Most ion sources generate beams with significant, and usually unknown, metastable fractions. This complicates and limits the ability both to generate reliable EII data and to benchmark theory. Experimental approaches that are particularly prone to this problem include crossed beams methods or merged electron–ion beams in a single-pass geometry (Müller 2008). In each arrangement, the metastable ions have insufficient time to radiatively relax to the ground state before the EII measurements are performed.

Additionally, a second issue arises from the need for EII cross sections for every astrophysically relevant ion, typically defined as all non-bare charge states of every element from H to Zn (e.g., Dere 2007). Limited experimental resources and personnel preclude being able to carry out all the required measurements.

In order to address these two issues, we have initiated a series of EII measurements employing an ion storage ring using a merged beams geometry. Utilizing a storage ring addresses the first issue by allowing for the ions to be stored long enough for typically all or nearly all metastable levels to radiatively relax before beginning data acquisition. To address the second issue, we have adopted the approach of measuring EII for at least one ion in every isoelectronic sequence. Our results can then be used to benchmark theory, which in turn can be used to calculate the needed EII data for other ions in the same isoelectronic sequence.

Boron-like was the first isoelectronic sequence selected for study. Here, we have investigated EII for B-like Mg^{7+} forming Be-like Mg^{8+}. Mg^{7+} peaks in abundance in an electron-ionized plasma at a temperature of about 8×10^5 K (Bryans et al. 2009). Spectral lines from this ion are observed in the solar corona (Curdt et al. 2004) and stellar spectra (Rasseen et al. 2002). The metastable lifetime of Mg^{7+} is several seconds. With storage times approximately an order of magnitude longer, this ion is particularly well suited for storage ring measurements of ground state EII. We then use our results here to benchmark theory.

Cross section measurements covered the center of mass energy range from 200 to 2000 eV. This energy range includes the following direct ionization channels:

$$e^- + Mg^{7+}(1s^2\,2s^2\,2p) \rightarrow \begin{cases} Mg^{8+}(1s^2\,2s^2) + 2e^- \\ Mg^{8+}(1s^2\,2s\,2p) + 2e^- \\ Mg^{8+}(1s\,2s^2\,2p) + 2e^- \end{cases} . \quad (1)$$

The energy thresholds for these channels are 265.96 eV, 283.37 eV, and 1587.32 eV, respectively (Ralchenko et al. 2008). In addition, above about 1291 eV there are excitation-autoionization (EA) channels from $1s\,2s^2\,2p\,nl$ excitation, leading to the first two configurations in Equation (1) (Safronova & Shlyaptseva 1996). Concerning ionization forming $Mg^{8+}(1s\,2s^2\,2p)$, the third configuration in Equation (1), this state radiatively stabilizes with a probability of <5% and otherwise autoionizes giving a net double ionization to form Mg^{9+} (Gorczyca et al. 2003). Here, we detect only the single ionization channel.

This paper is organized as follows. In Section 2, we describe the experimental setup. The data analysis is presented in Section 3 and uncertainties in Section 4. Experimental results and comparison to theory are presented in Section 5. A brief summary is given in Section 6.

2. EXPERIMENTAL SETUP

EII measurements were performed at the TSR heavy-ion storage ring of the Max-Plank-Institut für Kernphysik in Heidelberg, Germany. The experiments basically followed the procedure of previous experiments (Kilgus et al. 1992; Linkemann et al. 1995a; Kenntner et al. 1995; Schippers et al. 2001; Lestinsky et al. 2009). Here, we describe additional details relevant to the present work.

A beam of 80 MeV $^{24}Mg^{7+}$ ions was injected into TSR in a series of 1–3 pulses, typically 0.5 s apart. In one of the straight sections of TSR, the ion beam was merged with a beam of electrons in the electron cooler. The two beams co-propagated and interacted for a distance of ≈1.5 m. During injection the electron energy was 1816.6 eV, accounting for space charge corrections based on the electron current and the geometry of the cooler as described in Kilgus et al. (1992). This energy is denoted as the cooling energy. It resulted in a small relative velocity between the electrons and ions, which allowed the ion beam to be cooled efficiently by the electrons and set the ion velocity to that of the electrons at cooling. The resulting center of mass energy spread at cooling was well described by a flattened Maxwellian distribution with temperatures in the perpendicular and parallel directions of $k_B T_\perp = 13.5$ meV and $k_B T_\parallel = 180\ \mu$eV, respectively. These were determined from the widths of resonances in the dielectronic recombination (DR) spectrum (M. Lestinsky et al. 2010, in preparation). After injection the ions were cooled for 4.5–6 s, allowing the Mg^{7+} metastable states to decay. The $2s\,2p^2\,^4P_{\{1/2,3/2,5/2\}}$ levels decay with lifetimes of <0.1 ms and contribute to the population of the $2s^2\,2p\ ^2P_{3/2}$ level, which has a lifetime of ≈ 3.1 s. Based on the transition rates and branching ratios, and assuming an initial Boltzmann-distributed level population within the $n = 2$ shell, the average metastable fraction during measurement was estimated to be about 3% (M. Lestinsky et al. 2010, in preparation). The stored ion current after cooling was 2–8 μA.

Ionization and recombination were measured simultaneously using separate detectors located behind the first dipole magnet downstream of the electron cooler. Ions that underwent ionization were deflected more strongly than the Mg^{7+} beam, striking a converter plate, and generating secondary electrons which were then detected by a channel electron multiplier (CEM; Rinn et al. 1982; Linkemann et al. 1995b). Similarly, ions that underwent recombination were deflected less strongly than the Mg^{7+} beam and collected by a scintillation crystal (Miersch et al. 1996). The detectors were positioned for maximum signal collection by stepping each unit horizontally and vertically in small increments across each product beam. From these scans, we also determined that the cooled ion beam was about 1 mm in diameter, which is small compared to the 10 mm circular diameter opening of the ionization detector or to the 20 mm × 20 mm area of the recombination detector. Using a beam profile monitor (Hochadel et al. 1994), we observed that the beam diameter increases to about 4 mm during measurement as the beam warms up. This can cause a small decrease in the detection efficiency as is discussed in Section 4.

A suitable CEM discriminator level was determined by measuring the pulse height distribution. The level was set so that the detection efficiency of ionization events was essentially unity. The total ionization detector count rate was kept below ≲60 kHz by adjusting the electron beam current. The dead time of the ionization detector was estimated from the length of the CEM pulse to be about 30 ns, giving an upper limit for the dead-time-induced loss of 0.2%.

Data collection was performed by repeating a sequential cycle consisting of injection, cooling, and then energy scans. Each energy scan consisted of ∼50 pairs of steps, one step at measurement and one at reference. The laboratory electron energies were always chosen to be higher than the cooling energy and were between 3200 and 8100 eV. The higher energy ranges required large changes in the acceleration voltage between the cooling step and the energy scan. A fast high-voltage amplifier with a ±1000 V dynamic range was used for the energy scan in combination with a slower principal electron beam power supply, which was used to lift the fast amplifier into the range of the energy scan following the cooling phase. At the beginning of each scan step a short delay, typically 50–100 ms, allowed the power supplies to settle. Data at each step were then collected for 50–100 ms. The measurement energy was scanned over a range of about 600 V in the laboratory frame. A typical scan required 10–20 s.

The background count rate was determined by measuring the count rate at a fixed relative energy during the reference step. For lower energy scans the reference step energy was set below the EII threshold so that the background ionization count rate was due only to stripping of electrons off the residual gas (RG). However, at higher energies it was not possible to set the reference energy below threshold. This is because of the limited range of the fast high-voltage amplifier used to set the electron beam energy. Instead the reference step was set to an energy where the EII cross section could be determined from the lower energy scans. In this way, the EII contribution to the reference count rate could be removed in order to determine the appropriate background count rate for subtraction. We describe in detail in the next section the steps necessary to derive the appropriate background count rate, valid at the measurement step energy, from the reference rate at the fixed energy.

After an energy scan was complete a new injection cycle was initiated and the process repeated. Scans over a particular energy range were typically repeated for 1 hr to ensure good statistical accuracy. The energy range for each scan was chosen to maintain at least 50% overlap with other scans.

3. DATA ANALYSIS

The energy-dependent ionization cross section at each measured energy $\sigma_I(E_m)$ was obtained from the measured ionization rate coefficient $\langle\sigma_I v_{rel}\rangle$ which is averaged over the energy spread of the experiment. Because the relative velocity spread is very small, $\Delta v_{rel} \ll v_{rel}$, the averaged rate coefficient can be divided by the relative velocity giving

$$\sigma_I(E_m) = \frac{1}{v_{rel}}\left[\frac{R_I^m(E_m) - R_I^b(E_m)}{(1-\beta_i\beta_e)n_e^m N_i^m L} + \langle\sigma_I v_{rel}\rangle(E_r)\frac{n_e^r}{n_e^m}\right]. \quad (2)$$

Here, R_I^m denotes the total ionization count rate at the measurement step; R_I^b denotes the background ionization count rate at the measurement step, which is proportional to the count rate at the reference step R_I^r, as described below; $L = 1.5$ m is the length of the interaction region; the factor $(1 - \beta_i\beta e)$ is a relativistic correction, where β_i and β_e are the ion and electron velocities normalized by the speed of light, v_i/c and v_e/c, respectively; and E_m and E_r are the center of mass energies at measurement and reference, respectively. The electron density n_e is calculated from the measured electron current and the geometry of the electron cooler by assuming a uniform electron density (Kilgus et al. 1992). The electron density was typically on the order of 10^7 cm^{-3}. The total number of stored ions per unit length N_i is calculated from the measured ion current. The EII rate coefficient at the reference energy $\langle\sigma_I v_{rel}\rangle(E_r)$ is included in order to remove the EII contribution to the background count rate R_I^b when the reference energy is above the EII threshold. The factor n_e^r/n_e^m accounts for the different electron densities at reference and measurement.

The electron and ion beams also interact in the merging and demerging sections on either side of the straight section.

In this section, the ion and electron beams meet at an angle and the center of mass energy is greater than in the section where the beams are collinear. These toroidal effects from the merging and demerging of the beams are accounted for using the method described by Lampert et al. (1996). For a given collision energy the toroidal correction procedure requires knowledge of the cross section at energies up to 140 eV higher. At the highest measured energies an extrapolation was needed to supply cross section values so the correction could be applied. The extrapolation was obtained by fitting the experimental data using the Lotz formula (Lotz 1969). Over the entire scan range, this procedure corrects what would otherwise be an overestimate of the EII cross section by about 20% on average. This is mainly because the toroidal sections increase the effective length of the interaction region by about 20%.

The total ionization detector signal at the measurement step is made up of EII and electron stripping (ES) of the ions off the RG atoms,

$$R_{\rm I}^{\rm m}(E_{\rm m}) = \langle \sigma_{\rm I} v_{\rm rel} \rangle \, n_{\rm e}(E_{\rm m}) N_{\rm i}^{\rm m} L + \langle \sigma_{\rm ES} v_{\rm i} \rangle \, n_{\rm RG}(E_{\rm m}) N_{\rm i}^{\rm m} D. \quad (3)$$

Here, $n_{\rm RG}$ is the density of the RG, D is the length along the beam from which ions created by ES can reach the ionization detector, and $\sigma_{\rm ES}$ is the cross section for ES. To calculate the EII cross section, the background rate

$$R_{\rm I}^{\rm b}(E_{\rm m}) = \langle \sigma_{\rm ES} v_{\rm i} \rangle \, n_{\rm RG}(E_{\rm m}) N_{\rm i}^{\rm m} D \quad (4)$$

must be subtracted from $R_{\rm I}^{\rm m}(E_{\rm m})$. This background rate can be determined by measuring the count rate at a reference energy. We first consider the case where the reference energy $E_{\rm r}$ is below the EII threshold. To solve for $R_{\rm I}^{\rm b}(E_{\rm m})$, we note that in this case $\sigma_{\rm I}(E_{\rm r}) = 0$ and the reference count rate results exclusively from stripping giving

$$R_{\rm I}^{\rm r}(E_{\rm r}) = \langle \sigma_{\rm ES} v_{\rm i} \rangle \, n_{\rm RG}(E_{\rm r}) N_{\rm i}^{\rm r} D. \quad (5)$$

Taking the ratio of Equations (4) and (5) and solving for $R_{\rm I}^{\rm b}(E_{\rm m})$, one obtains

$$R_{\rm I}^{\rm b}(E_{\rm m}) = \left[\frac{n_{\rm RG}(E_{\rm m})}{n_{\rm RG}(E_{\rm r})} \frac{N_{\rm i}^{\rm m}}{N_{\rm i}^{\rm r}} \right] R_{\rm I}^{\rm r}(E_{\rm r}). \quad (6)$$

This equation corrects for the fact that the count rate at reference $R_{\rm I}^{\rm r}(E_{\rm r})$ is not exactly equal to the background rate at the measurement step $R_{\rm I}^{\rm b}(E_{\rm m})$. The RG density $n_{\rm RG}$ and the number of stored ions per unit length $N_{\rm i}$ can differ between each step. In particular, increasing the electron energy increases the electron current which can change the gas pressure in the vacuum system. Also, the number of ions in the interaction region varies between the measurement and reference steps because of the exponential decay of the stored ion beam, which here had a characteristic decay time of $\approx$30 s. This implies an offset between the reference rate and the background rate at the measurement step measured 50–100 ms later (or earlier) of about 0.5%. Both these effects can be a source of systematic error and are hence corrected, as far as possible, as described below.

For energy ranges with a reference $E_{\rm r}$ where $\sigma_{\rm I} = 0$, we can determine the prefactor on the right-hand side of Equation (6) by simultaneously measuring electron–ion recombination. At the high energies of interest for EII, the recombination signal at both measurement $R_{\rm R}^{\rm m}$ and reference $R_{\rm R}^{\rm r}$ is dominated by electron capture (EC) off the RG with a component due to electron–ion recombination in the cooler. That is,

$$R_{\rm R}^{\rm m}(E_{\rm m}) = \langle \sigma_{\rm rec} v_{\rm rel} \rangle \, n_{\rm e}(E_{\rm m}) N_{\rm i}^{\rm m} L + \langle \sigma_{\rm EC} v_{\rm i} \rangle \, n_{\rm RG}(E_{\rm m}) N_{\rm i}^{\rm m} D \quad (7)$$

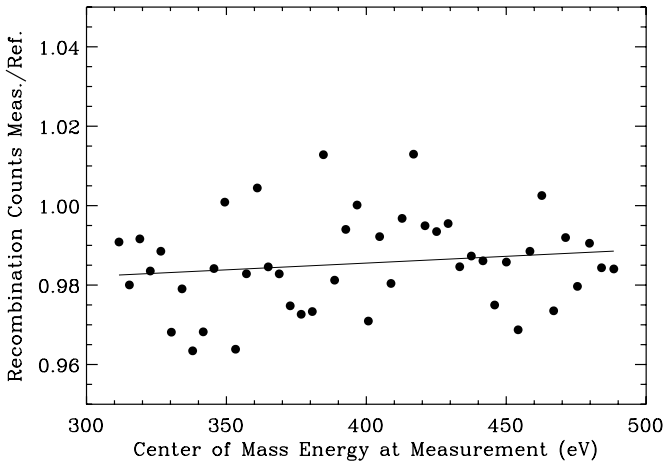

Figure 1. Shown here is the ratio given by Equation (9). This ratio shows an offset due primarily to the decay of the ion beam between measurement and reference steps, and a slope due to the changing RG pressure as a function of energy. The linear fit shown is used to correct the ionization signal reference rate $R_{\rm I}^{\rm r}(E_{\rm r})$ in order to obtain the background rate at measurement $R_{\rm I}^{\rm b}(E_{\rm m})$.

and

$$R_{\rm R}^{\rm r}(E_{\rm r}) = \langle \sigma_{\rm rec} v_{\rm rel} \rangle \, n_{\rm e}(E_{\rm r}) N_{\rm i}^{\rm r} L + \langle \sigma_{\rm EC} v_{\rm i} \rangle \, n_{\rm RG}(E_{\rm r}) N_{\rm i}^{\rm r} D. \quad (8)$$

Here, $\sigma_{\rm EC}$ is the cross section for EC and $\sigma_{\rm rec}$ is the cross section from the sum of radiative recombination and DR. The electron–ion component of the total recombination signal is removed using separate measurements of $\sigma_{\rm rec}$ made with the reference energy chosen using the criterion that the electron–ion contribution at that point be close to zero (M. Lestinsky et al. 2010, in preparation). Using Equations (7) and (8), the ratio of gas densities and ion numbers can now be expressed in terms of these quantities measured in the recombination channel,

$$\frac{n_{\rm RG}(E_{\rm m})}{n_{\rm RG}(E_{\rm r})} \frac{N_{\rm i}^{\rm m}}{N_{\rm i}^{\rm r}} = \frac{R_{\rm R}^{\rm m}(E_{\rm m}) - \langle \sigma_{\rm rec} v_{\rm rel} \rangle \, n_{\rm e}(E_{\rm m}) N_{\rm i}^{\rm m} L}{R_{\rm R}^{\rm r}(E_{\rm r}) - \langle \sigma_{\rm rec} v_{\rm rel} \rangle \, n_{\rm e}(E_{\rm r}) N_{\rm i}^{\rm r} L}. \quad (9)$$

An example is shown in Figure 1. Substituting this expression into Equation (6) gives

$$R_{\rm I}^{\rm b}(E_{\rm m}) = \frac{R_{\rm R}^{\rm m}(E_{\rm m}) - \langle \sigma_{\rm rec} v_{\rm rel} \rangle \, n_{\rm e}(E_{\rm m}) N_{\rm i}^{\rm m} L}{R_{\rm R}^{\rm r}(E_{\rm r}) - \langle \sigma_{\rm rec} v_{\rm rel} \rangle \, n_{\rm e}(E_{\rm r}) N_{\rm i}^{\rm r} L} R_{\rm I}^{\rm r}(E_{\rm r}). \quad (10)$$

This correction ensures that the background level from ES is proportional to the energy-dependent RG pressure and the ion current during the measurement step. An example of this correction is shown in Figure 2 and its effect on the calculated EII cross section is illustrated in Figure 3.

The correction outlined here cannot be applied to measurements having a reference energy where $\sigma_{\rm I}(E_{\rm r}) \neq 0$ due to the need to include the EII rate in Equation (5). However, Equation (9) continues to be valid and we found experimentally that at these higher energies the ratio on the right-hand side of Equation (9) was compatible with a constant to within the statistical errors. Moreover, the ratio $N_{\rm i}^{\rm m}/N_{\rm i}^{\rm m}$ is always constant since the ion beam decays exponentially and the time interval between steps is fixed. Observing no significant variation of the ratio with energy and considering the fact that the only source of such a variation would be RG pressure fluctuations, we conclude that the RG pressure has saturated and we perform no correction. Hence, for those measurements only the effect of the ion beam decay was corrected for using direct measurements of the

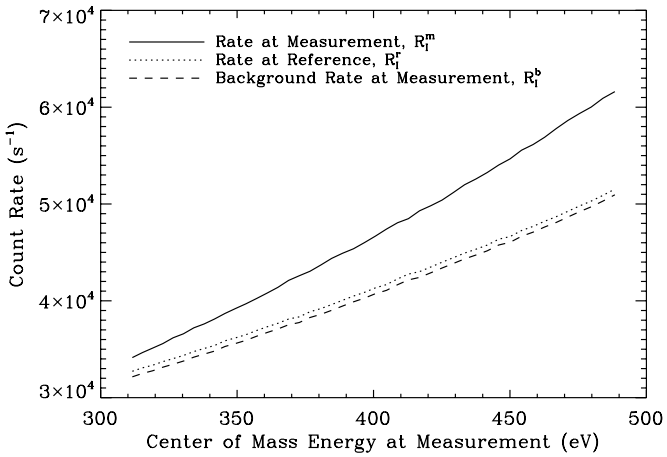

Figure 2. Count rate at the varying measurement energy $R_I^m(E_m)$ and the count rate at the fixed reference energy $R_I^r(E_r)$ are shown. Also shown is $R_I^b(E_m)$, the reference rate adjusted following Equation (10) using the fit in Figure 1. In this example, the measurement cycle scanned from high to low energy and the large slope in the measured rates is caused by the decreasing ion beam current over time. Since the reference rate is measured repeatedly each time E_m is varied, its apparent dependence on E_m is actually a time dependence caused by the decay of the ion beam.

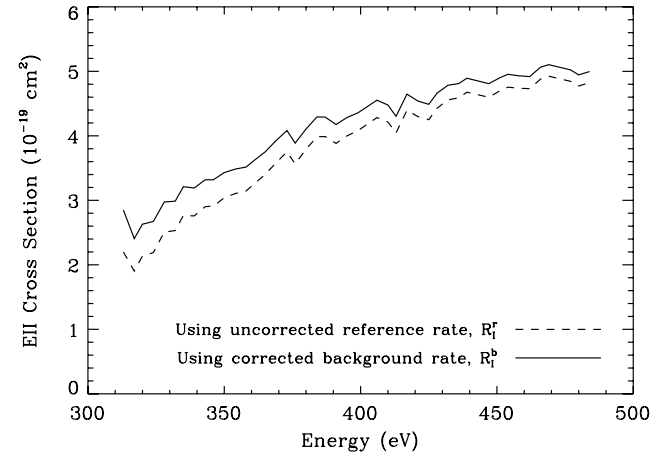

Figure 3. EII cross section calculated from the count rates shown in Figure 2. For this energy range there is a noticeable difference in the calculated cross section when the background rate corrected for pressure and ion decay $R_I^b(E_m)$ is used compared to when it is assumed the background rate equals the reference rate $R_I^r(E_r)$.

ion current. For the higher-energy scans with $\sigma_I(E_r) \neq 0$, the EII rate contribution included in the background rate $R_I^b(E_m)$ has to be removed by the second term in Equation (2), which in this experiment has been taken from the cross section determined in the scans at lower energies.

4. UNCERTAINTIES

Table 1 summarizes the errors arising from counting statistics and systematic sources. Because of the long times over which data were accumulated, the 1σ counting statistics results in uncertainties of less than 1%. The systematic error is primarily due to the 15% uncertainty of the stored ion beam current and uncertainties introduced by the heating of the ion beam phase space. The stored ion current is measured non-destructively with a DC beam current transformer (Unser 1981). The systematic error of the ion current, caused by these instrumental fluctuations, applies to each energy scan separately. Since the scans of higher energy are linked to the lower energy ones by the procedure

Table 1
Sources of Uncertainty

Source	Estimated Uncertainty (%)
Ion current measurement	15
Detection efficiency	2
Interaction length spread	1
Counting statistics	1
Quadrature sum	15

described at the end of Section 3, the relative comparison of cross sections at collision energies strongly different from each other can also be affected by an error of similar size as the ion current measurement; hence, in spite of a much better statistical error, we conservatively apply a 15% error band on the functional form of the cross section. The beam could not be cooled after the initial injection and cooling period because of the limited dynamic range (±1000 V) of the fast high-voltage amplifier used to scan the electron energy. Thus, after the initial cooling period, the ion beam warms up. Using a beam profile monitor (Hochadel et al. 1994) we found that the diameter expands within a few seconds from about 1 mm to about 4 mm as measured during the experiment. Because the beam expansion is time varying and may not be isotropic, we estimated the uncertainty rather than attempt to correct for it. By assuming a Gaussian beam and comparing with the diameter of the ionization detector we estimated the uncertainty in the detection efficiency due to the increase in beam size to be ≈2%. The uncertainty arising from inaccurate knowledge of the overlap length L is strongly reduced by the toroidal correction as described in Lampert et al. (1996). The expansion of the ion beam introduces a spread of $\lesssim$1% in the effective overlap length experienced by ions at different transverse locations. Treating the systematic errors as Gaussian uncertainties and adding them in quadrature, we estimate the 1σ total systematic uncertainty in the cross section to be 15%. The total error bar from adding the above uncertainties in quadrature is 15% and is dominated by the systematic uncertainty.

5. RESULTS AND DISCUSSION

Our experimental results are shown in Figure 4 for the full center of mass energy range from 200 to 2000 eV (corresponding to laboratory electron energies of 3200–8100 eV), while a more detailed view near the EII threshold energy is shown in Figure 5. In Figure 4, the error bars at selected points indicate the total 1σ experimental uncertainty of 15%. In Figure 5, the smaller error bars indicate the statistical uncertainty, which is more significant when the EII cross section is small because the count rates are low. The larger error bars in Figure 5 indicate the total 1σ experimental uncertainty. The thresholds for the different direct ionization channels described in Equation (1) are indicated by arrows in each figure. The observed EII threshold appears near the predicted value of 265.96 eV. The absence of any ionization signal below this threshold is an indication that the metastable fraction in the experiment is small. The threshold for the $2s$ ionization channel at 283.37 eV could not be observed experimentally.

For B-like ions the EA contribution to the ionization process is expected to be only a few percent of the direct ionization contribution to the cross section (Sampson & Golden 1981). The expected threshold for this indirect ionization mechanism is about 1291 eV (Safronova & Shlyaptseva 1996). Our experimental measurement did not resolve the EA contribution. We

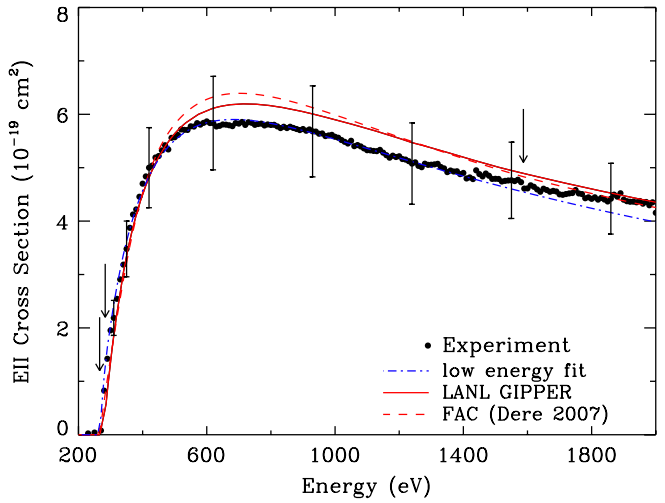

Figure 4. Electron impact ionization cross section for Mg^{7+} forming Mg^{8+} in the relative energy range 200–2000 eV. The estimated total 1σ experimental uncertainty is illustrated by error bars at selected points. Arrows are used to indicate the energy thresholds for the different ionization channels. The apparent structures in the experimental results near 600 eV, 1400 eV, and 1800 eV are due to run to run variations in the background levels. The dot-dashed line is a result of a fit to the experimental data below 1100 eV using the Lotz formula in order to illustrate the change of shape at high energies that may be caused by EA and the third ionization channel. Also shown are theoretical results from the LANL Atomic Code GIPPER and the FAC code.

(A color version of this figure is available in the online journal.)

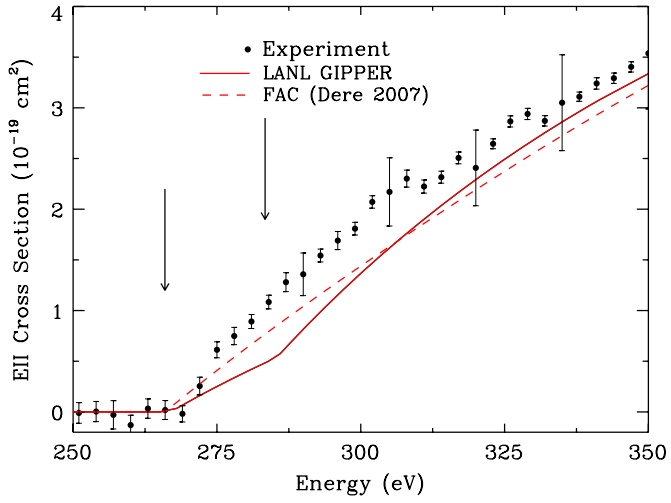

Figure 5. Electron impact ionization cross section for Mg^{7+} forming Mg^{8+} in the relative energy range 250–350 eV. The smaller error bars show the 1σ uncertainty arising from the counting statistics, while the larger error bars illustrate the total 1σ experimental uncertainty. The arrows indicate the energy thresholds for the ionization channels. The theoretical results from the LANL Atomic Code GIPPER and the FAC code are also shown.

(A color version of this figure is available in the online journal.)

do observe an apparent difference in the shape of the curve at high energies, but this is well within the experimental uncertainty. Our results are consistent with calculations and experimental measurements for other B-like ions which showed the EA contribution to be small (Yamada et al. 1989; Bannister 1997; Duponchelle et al. 1997; Chongyang et al. 1998; Loch et al. 2003). Additionally, we did not resolve contributions from indirect processes involving excitation of inner shell electrons by dielectronic capture followed by autoioinization, such as resonant excitation double autoionization or resonant excitation auto-double-ionization.

Also shown in Figures 4 and 5 are theoretical results from two different distorted wave calculations. One calculation was performed using the GIPPER code from the Los Alamos Atomic Physics Code suite (Magee et al. 1995). This total cross section is the sum of the three direct ionization channels in Equation (1). The other theoretical cross section was reported by Dere (2007) and was calculated using the FLEXIBLE ATOMIC CODE (FAC) code (Gu 2003). These results are the sum of the three direct ionization channels plus EA and have been incorporated into the CHIANTI database (Dere et al. 2009). To within the experimental uncertainties, our measured cross section is in agreement with both of these calculations. This agreement increases the confidence in the EII data for Mg^{7+} based on these codes and used in astrophysics.

6. SUMMARY

We have measured the EII cross section of Mg^{7+} using the TSR ion storage ring to produce an ion beam with an average estimated metastable fraction of ≈3%. The measured cross section agrees with theoretical distorted wave calculations to within the experimental uncertainties. This adds confidence to astrophysical measurements that rely on the atomic EII data for this ion.

The most significant limitation on these measurements is a systematic uncertainty in the ion current measurement. We plan to improve this situation in future measurements. To this end, we are now developing new methods to mitigate the effect of this uncertainty by correcting for fluctuations between energy scans, which will remove distortions of the functional shape of the cross section.

We gratefully acknowledge the efficient support by the accelerator and TSR groups during the beamtime. This work was supported in part by the NASA Astronomy and Physics Research and Analysis program and the NASA Solar Heliospheric Physics program.

REFERENCES

Bannister, M. E. 1997, Phys. Rev. A, 54, 1435
Brickhouse, N. S. 1996, in AIP Conf. Ser. 381, Atomic Processes in Plasmas (Tenth), ed. A. L. Osterheld & W. H. Goldstein (Melville, NY: AIP)
Bryans, P., Badnell, N. R., Gorczyca, T. W., Laming, J. M., Mitthumsiri, W., & Savin, D. W. 2006, ApJS, 167, 343
Bryans, P., Landi, E., & Savin, D. W. 2009, ApJ, 691, 1540
Chongyang, C., Shixiang, Y., Zhouxuan, T., Yansen, W., Fujia, Y., & Yongsheng, S. 1998, J. Phys. B: At. Mol. Opt. Phys., 31, 2667
Curdt, W., Landi, E., & Feldman, U. 2004, A&A, 427, 1045
Dere, K. P. 2007, A&A, 466, 771
Dere, K. P., Landi, E., Young, P. R., Del Zanna, G., Landini, M., & Mason, H. E. 2009, A&A, 498, 915
Duponchelle, M., Khouilid, M., Oualim, E. M., Zhang, H., & Defrance, P. 1997, J. Phys. B: At. Mol. Opt. Phys., 30, 729
Gorczyca, T. W., et al. 2003, ApJ, 592, 636
Gu, M. F. 2003, ApJ, 582, 1241
Hochadel, B., Albrect, F., Grieser, M., Schwalm, D., Szmola, E., & Wolf, A. 1994, Nucl. Instrum. Methods A, 343, 401
Kenntner, J., et al. 1995, Nucl. Instrum. Methods B, 98, 142
Kilgus, G., Habs, D., Wolf, A., Badnell, N. R., & Müller, A. 1992, Phys. Rev. A, 46, 5730
Lampert, A., Wolf, A., Habs, A., Kenntner, J., Kilgus, G., Schwalm, D., Pindzola, M. S., & Badnell, N. R. 1996, Phys. Rev. A, 53, 1413
Landi, E., & Landini, M. 1999, A&A, 347, 401
Lestinsky, M., et al. 2009, ApJ, 698, 648
Linkemann, J., Müller, A., Kenntner, J., Habs, D., Schwalm, D., Wolf, A., Badnell, N. R., & Pindzola, M. S. 1995a, Phys. Rev. Lett., 74, 4173

Linkemann, J., et al. 1995b, Nucl. Instrum. Methods B, 98, 154
Loch, S. D., Colgan, J., Pindzola, M. S., Westermann, M., Scheuermann, F., Aichele, K., Hathiramani, D., & Salzborn, E. 2003, Phys. Rev. A, 67, 042714
Lotz, W. 1969, Z. Phys., 220, 466
Magee, N. H., et al. 1995, in ASP Conf. Ser. 78, Astrophysical Applications of Powerful New Databases, ed. S. J. Adelman & W. L. Wiese (San Francisco, CA: ASP), 51 (http://aphysics2.lanl.gov/tempweb/)
Miersch, G., Habs, D., Kenntner, J., Schwalm, D., & Wolf, A. 1996, Nucl. Instrum. Methods A, 369, 277
Müller, A. 2008, in Advances in Atomic, Molecular, and Optical Physics, Vol. 55, ed. E. Arimondo, P. Berman, & C. Lin (London: Elsevier), 293
Ralchenko, Y., et al. 2008, NIST Atomic Spectra Database (Gaithersburgh, MD: National Institute of Standards and Technology), http://physics.nist.gov/asd3
Rasseen, A. J. J., et al. 2002, A&A, 389, 228
Rinn, K., Müller, A., Eichenauer, H., & Salzborn, E. 1982, Rev. Sci. Instrum., 53, 829
Safronova, U. I., & Shlyaptseva, A. S. 1996, Phys. Scr., 54, 254
Sampson, D. H., & Golden, L. B. 1981, J. Phys. B: At. Mol. Phys., 14, 903
Schippers, S., Müller, A.and Gwinner, G., Linkemann, J., Saghiri, A. A., & Wolf, A. 2001, ApJ, 555, 1027
Unser, K. 1981, IEEE Trans. Nucl. Sci., 28, 2344
Yamada, I., et al. 1989, J. Phys. Soc. Japan, 58, 1585